THERMAL RADIATION FROM A NUCLEAR WEAPON BURST

R. D. Small and H. L. Brode

Pacific-Sierra Research Corporation
12340 Santa Monica Boulevard
Los Angeles, California 90025

ABSTRACT

The different methods and correlations used to calculate the propagation of thermal radiation are reviewed and compared. A simple method to account for radiation enhancement by reflection from a superior cloud deck or snow cover, as well as attenuation of radiation by cloud cover below the burst is presented. The results show that the thermal "reach" may vary considerably. Additional calculations show that a significant fraction of the thermal energy may be incident after the arrival of the shock wave. Results for a range of weapon yields are presented, and the implications for blast-induced (secondary) fire starts are discussed.

INTRODUCTION

Approximately 35 to 45% of the energy from a nuclear weapon explosion is emitted as thermal radiation. Materials exposed to the fireball may be subject to a rapid increase in temperature. Flammable objects may ignite. The rapid heating of structural materials lowers the effective yield stress and in extreme cases can cause failure of load bearing elements. Lesser heating levels may lead to structure degradation or failure when combined with the subsequent shock wave loading. Low thermal flux levels can damage focussing optical devices that image the nuclear fireball. Retinal eye damage and skin burns occur at very low levels of incident thermal radiation.

In this paper, we review the basic relations describing the calculation of thermal flux from a nuclear fireball and consider some effects that modify the results. A short calculation illustrating the partition of incident energy before and after the shock wave arrival is presented. The results are relevant to the prediction of thermally and blast induced ignitions, shock precursor calculations, and structural response.

THERMAL PULSE

Thermal output from the fireball occurs in two pulses. The time interval of the first pulse is limited by the early shock wave formation (opaque fireball) and only a small fraction of the total energy is emitted. Following the shock breakaway, the fireball is again visible and the major fraction of energy is radiated. The rise to maximum energy output for the first pulse occurs in a few milliseconds and that for the second pulse in hundreds of milliseconds. The following correlations describe the early pulse characteristics as a function of weapon yield W (in kt) and burst altitude to sea-level density ratio η (1):

$$\text{time to first maximum} \simeq 0.10 W^{1/3} \eta^{0} \text{ msec} \tag{1}$$

$$\text{time to minimum} \simeq 3.8 W^{2/5} \eta^{0} \text{ msec} \pm 35\% \tag{2}$$

$$\text{time to second maximum} \simeq 50W^{0.2}\eta^{0.42} \text{ msec} \pm 20\% \ . \tag{3}$$

Since the initial pulse is short and contributes little to the total energy release, it is sufficient in most applications to consider the output from the second pulse only. Relations characterizing the time to maximum t_{max}, power maximum P_{max}, and pulse shape P/P_{max}, developed from fits to atmospheric test data and detailed radiation-hydrodynamics calculations (1) through (5) are:

$$t_{max} \simeq 0.05W^{0.42} \text{ sec} \pm 20\% \tag{4}$$

$$P_{max} \simeq 4.5W^{0.6}\eta^{-0.42} \text{ kt/sec} \pm 40\% \tag{5}$$

$$P/P_{max} \simeq \frac{2t^{*2}}{1 + t^{*4}} \ , \quad t^* = t/t_{max} \ . \tag{6}$$

The pulse shape agrees well with that presented by Glasstone and Dolan (6), though the late decay to zero energy output is probably too slow.

THERMAL ENERGY OUTPUT

One method to relate the thermal output to the total weapon energy is through the use of a partition function, f. The total energy available as thermal radiation is thus

$$E_{TH} = f W \ . \tag{7}$$

For visible and infrared radiations from airbursts, Brode (1) suggests the following form for the thermal partition function

$$f = 0.27 + 0.06\eta + \frac{114\eta}{82{,}000\eta^2 + 1} + \frac{0.0085\sqrt{W}}{1 + 0.032\sqrt{W}} \pm 20\% \tag{8}$$

η is the altitude to sea-level density ratio and W is the yield in kt. f increases from 0.35 for heights of burst less than 4500 m to 0.45 for heights of burst greater than 30,000 m.

For surface bursts, the thermal output is complicated by the distorted geometry of the fireball, by the materials engulfed and vaporized within the fireball, and by the obscuration due to dust and smoke clouds raised outside the fireball. For megaton bursts, the output at points on or near the ground from surface bursts is about half that from airbursts, i.e., less than 20% of the total yield.

The emitted thermal energy fraction (for air bursts) can be obtained as a function of time from the following integral of the power spectrum

$$E/E_{TH} = \frac{\sqrt{2}N}{\pi} \int_0^{t^*} P/P_{max} dt^* \ , \tag{9}$$

where N varies with t* as

$$N = 1 - 0.283e^{-1.181/t^*} \quad , \quad t^* \leq 2.5 \tag{10}$$

$$N = 1 - 0.2e^{-0.05t^*} \quad , \quad t^* \geq 2.5 \quad . \tag{11}$$

The coefficient $\sqrt{2}N/\pi$ normalizes the energy fraction to 80% at $t/t^* = 10$. From Eqs. (6), (7) and (9) the thermal energy output as an explicit function of time is

$$E = fW \frac{N}{\pi} \left\{ \text{arctg}\,(\sqrt{2}t^* - 1) + \text{arctg}\,(\sqrt{2}t^* + 1) - \frac{1}{2} \ln\left(\frac{1 + \sqrt{2}t^* + t^{*2}}{1 - \sqrt{2}t^* + t^{*2}}\right) \right\} kt \quad . \tag{12}$$

INCIDENT THERMAL FLUX

The energy flux decreases proportionately with the square of the slant range $\tilde{R}$(km), and as a function of time the incident thermal flux is approximated as

$$Q = 10^{12}\, ET/4\pi\tilde{R}^2 \ \text{cal/cm}^2 \quad . \tag{13}$$

For W in kt and $\tilde{R}$ in miles, the total energy output reduces to

$$Q_{TH} = WT/\tilde{R}^2 \ \text{cal/cm}^2 \quad . \tag{14}$$

The transmissivity T accounts for the scattering and absorption of radiation in the atmosphere. In general, scattering increases the transmissivity linearly with range, and the absorption decreases T exponentially. Analytic fits to experimental data (Fig. 1) indicate a relationship of the form

$$T = \left(1 + \alpha\frac{\tilde{R}}{V}\right)e^{-\beta\tilde{R}/V} \quad , \tag{15}$$

where V is the visibility length and α and β specify the degree of atmospheric scattering and absorption of the radiation. The visibility length characterizes the state of the atmosphere and varies from 280 m for an exceptionally clear day to less than 1 km for a light-to-thick fog. A clear day is defined as V = 20 m (6). Recommended values for α, β vary from 1.4, 2.0 (1, 6) to 1.9, 2.9 (7). The influence of visibility length and transmissivity form on the effective thermal reach for a 1 Mt burst is illustrated in Fig. 2.

The amount of radiant energy incident on a target can be modified by the presence of cloud cover above or below the burst, and by ground snow cover. Simple estimates can be made using multiplicative factors. For example, a lower cloud deck (below the burst) reduces the energy arrival so that

$$Q_{effective} = \sigma\, 10^{12}\, ET/4\pi\tilde{R}^2 \ \text{cal/cm}^2 \quad , \tag{16}$$

where σ is less than 1.0. Radiation enhancement due to reflection from a superior cloud deck or snow cover may also be calculated from Eq. (16) using

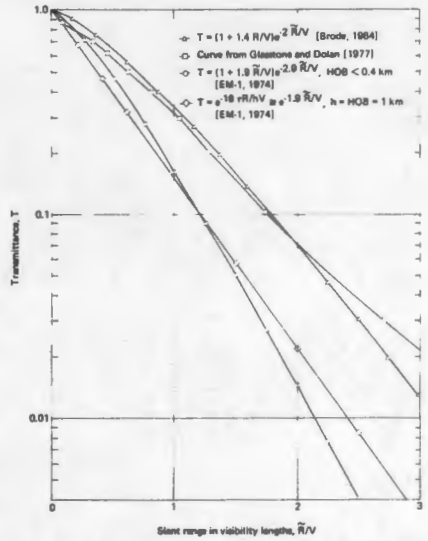

Fig. 1 Standard forms for calculating total visible radiation from airblast

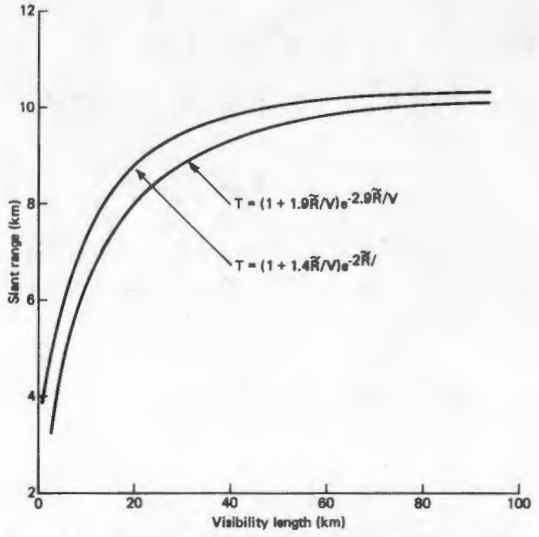

Fig. 2 Slant range vs. visibility length for 1 Mt burst, 152 m scaled height of burst and incident flux level of 22 cal/cm^2

values of σ greater than 1.0 but less than 2. The potential change in thermal reach is illustrated in Fig. 3 for a range of attenuation and enhancement factors. For $0.25 \leq \sigma \leq 1.9$, the thermal reach increases by 30% or decreases by 50% from the nominal $\sigma = 1.0$.

LATE THERMAL RADIATION

As the weapon yield increases, the thermal pulse lasts longer and a significant fraction of the radiation may be incident after the shock wave arrival. For scaled ground ranges less than 0.5 kft/kt$^{1/3}$, more than half the thermal energy may arrive after the shock wave. At greater ranges (e.g., 1-5 kft/kt$^{1/3}$) 5 to 20% of the thermal energy follows the shock arrival. The latter values may correspond to low overpressure regions (less than 5 psi). Sufficient energy is available to ignite materials exposed by the blast disruption as well as contribute to the spectra of "secondary" ignitions.

The partition of energy arriving before and after the shock wave may be calculated using Eqs. (10) through (15) once the shock time of arrival is specified. This time can be conveniently calculated from the following analytic fit developed by Brode (8)

$$\text{time of arrival} = W^{1/3}\,\frac{0.54291 - 21.185R^* + 361.8R^{*2} + 2383R^{*3}}{1 + 2.048R^* + 2.6872R^{*2}}\ \text{msec} \quad . \qquad (17)$$

The weapon yield, W, is in kt and R* is the scaled slant range in kft/kt$^{1/3}$.

A sample calculation illustrating the energy fraction incident on a target after the shock arrival as a function of weapon yield and scaled ground range is shown in Fig. 4. The influence of the fixed (2.5 kft) height of burst is evident at zero ground range. Close to ground zero, most of radiation arrives after the shock wave for weapon yields larger than 1 Mt. This suggests that even in heavily blast damaged areas, many thermal ignitions will occur. At greater ranges, the amount of late thermal decreases rapidly, though remains significant out to about 3.5 kft/kt$^{1/3}$. For this calculation, the thermal flux corresponding to $E/E_{TH} \sim 0.2$ was 10 cal/cm^2.

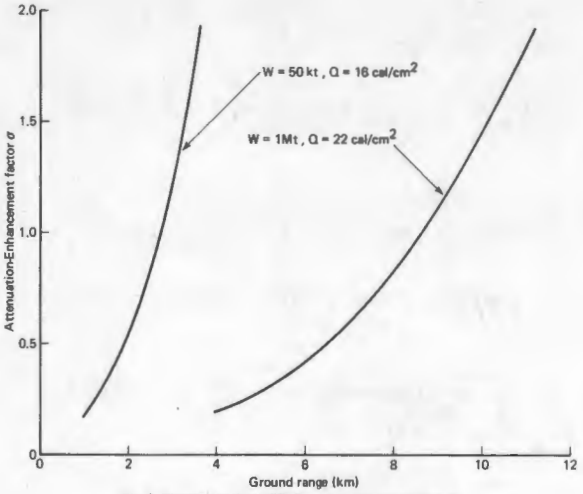

Fig. 3 Thermal reach modified by radiation attenuation or enhancement: SHOB = 152m, V = 19.3 km, $T = (1 + 1.4R/V)\, e^{-2R/V}$

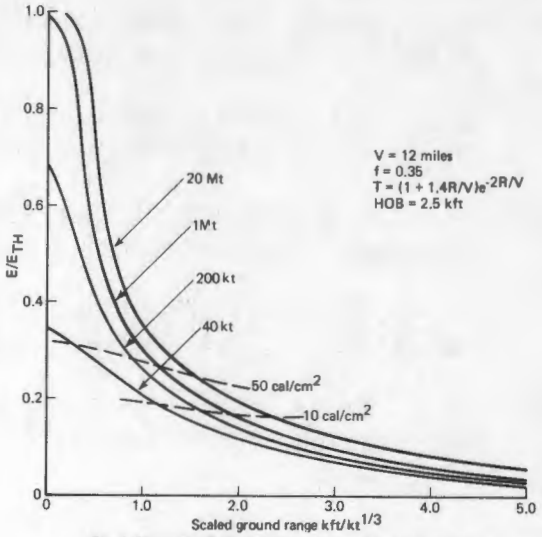

Fig. 4 Thermal radiation fraction incident after shock arrival vs. scaled ground range

SUMMARY AND CONCLUSIONS

The relations presented in this paper for calculation of thermal energy fluxes are based on analysis of weapons tests and detailed radiation-hydrodynamics computations. Many of the analytic forms have uncertainties of 20% or greater. Though atmospheric testing may not be possible, uncertainties involving visibility lengths and transmissivity may be reduced in a test series using high powered light sources. Additional experiments may define the degrees of radiation enhancement and attenuation by snow and cloud cover.

The influence of transmissivity form, visibility length, and reflection or absorption of fireball radiation was explored. Either singly or in combination, these parameters can significantly modify the level of incident thermal radiation. Perturbations about probable values can be used to indicate deviations from expected flux levels. A sample calculation showed that a major fraction of the thermal flux can arrive at a target after the shock wave. Synergistic effects of late thermal and blast disruption may increase the number of "secondary" fire starts.

Analysis of incipient ignitions, fire start distributions, shock precursors, transient thermal loading of structural elements, and personnel casualties depends on the rate and level of incident thermal energy deposition. The functions presented in this note facilitate those calculations.

REFERENCES

1. H. L. Brode, "Review of Nuclear Weapons Effects," Annual Review of Nuclear Science, Vol. 18, pp. 153-202 (1968).

2. H. L. Brode, Fireball Phenomenology, The Rand Corporation, Santa Monica, California, P3026 (1964), (paper presented at the Tripartite Technical Cooperation Panel Meeting, Panel N3, Dorking, England, October 1964).

3. H. L. Brode, Theoretical Description of the Blast and Fireball for a Sea Level Kiloton Explosion, The Rand Corporation, Santa Monica, California, RM2246PR (1966).

4. H. L. Brode, "Gas Dynamic Motion with Radiation: A General Numerical Method," Astronautica Acta, Vol. 14, pp. 433-444 (1969).

5. R. W. Hillendahl, Theoretical Models for Nuclear Fireballs, Lockheed Missile and Sapce Company, DASA 1589 (1965).

6. S. Glasstone and S. J. Dolan, The Effects of Nuclear Weapons, 3rd ed. U.S. Department of Defense and the U.S. Department of Energy (1977).

7. -----, Capabilities of Nuclear Weapons, Defense Nuclear Agency Effects Manual No. 1, DNA-EM-1(N) (November 1974).

8. H. L. Brode, Height of Burst Effects at High Overpressures, The Rand Corporation, Santa Monica, California, DASA 2506 (July 1970).